GENETICS

N-terminal acetylation of Set1-COMPASS fine-tunes H3K4 methylation patterns

Hyeonju Woo[1]†, Junsoo Oh[2]†, Yong-Joon Cho[2,3], Goo Taeg Oh[1], Seon-Young Kim[4], Kisoon Dan[5], Dohyun Han[5,6,7], Jung-Shin Lee[2]*, TaeSoo Kim[1]*

H3K4 methylation by Set1-COMPASS (complex of proteins associated with Set1) is a conserved histone modification. Although it is critical for gene regulation, the posttranslational modifications of this complex that affect its function are largely unexplored. This study showed that N-terminal acetylation of Set1-COMPASS proteins by N-terminal acetyltransferases (NATs) can modulate H3K4 methylation patterns. Specifically, deleting NatA substantially decreased global H3K4me3 levels and caused the H3K4me2 peak in the 5′ transcribed regions to shift to the promoters. NatA was required for N-terminal acetylation of three subunits of Set1-COMPASS: Shg1, Spp1, and Swd2. Moreover, deleting Shg1 or blocking its N-terminal acetylation via proline mutation of the target residue drastically reduced H3K4 methylation. Thus, NatA-mediated N-terminal acetylation of Shg1 shapes H3K4 methylation patterns. NatB also regulates H3K4 methylation, likely via N-terminal acetylation of the Set1-COMPASS protein Swd1. Thus, N-terminal acetylation of Set1-COMPASS proteins can directly fine-tune the functions of this complex, thereby substantially shaping H3K4 methylation patterns.

INTRODUCTION

Histones undergo posttranslational modifications, including acetylation, methylation, phosphorylation, and ubiquitination, that are important for regulating chromatin structure and transcription by RNA polymerase II (RNA Pol II) (*1*, *2*). In particular, histone acetylation disrupts the interaction between histone and DNA, which opens up the chromatin, thereby facilitating RNA Pol II–mediated transcription (*3*–*5*). By contrast, histone methylation does not directly affect chromatin structure; rather, it serves as binding sites for downstream effectors that shape transcription in varying ways (*2*).

Histone methylation mainly occurs at the lysine residues of histones by adding one (mono, me1), two (di, me2), or three (tri, me3) methyl groups by histone methyltransferases. Cotranscriptional histone H3 methylation at K4 is mediated by the Set1-COMPASS (complex of proteins associated with Set1), which is the only H3K4 methyltransferase complex in budding yeast (*6*–*8*). Set1-COMPASS consists of the catalytic component Set1 and seven accessory proteins, namely, Swd3/Cps30, Swd1/Cps50, Bre2/Cps60, Sdc1/Cps25, Spp1/Cps40, Swd2/Cps35, and Shg1/Cps15 (*6*, *7*). By contrast, mammals have multiple complexes. In particular, humans have six (*6*–*8*), each of which bears a Set1-like catalytic subunit (Set1A, Set1B, and MLL1-MLL4), a core of four common components (WDR5, RbBP5, Ash2L, and DPY30) that is designated WRAD and interacts with the catalytic domain, and additional subunits that are specific for each complex (*9*, *10*). In Set1-COMPASS, the WRAD complex is composed of Swd3 (the yeast equivalent of WDR5), Swd1 (RbBP5), Bre2 (Ash2L), and Sdc1 (DPY30) (*11*, *12*). The fifth COMPASS protein, Spp1, binds to the nSET domain of Set1, which is located next to the N terminus of the SET domain and is important for H3K4me3 (*12*). Relatively little is known about Shg1. The Set1-COMPASS complex specifically associates with actively transcribed genes by interacting with the phosphorylated C-terminal domain of Rpb1, which is the largest subunit of RNA Pol II (*13*, *14*). Consequently, the transcription start sites (TSSs) of active genes are enriched for H3K4me3 and Set1. By contrast, H3K4me2 is prominently found at the 5′ regions of transcribed genes, and H3K4me1 is observed at the 3′ regions (*1*). This canonical pattern of H3K4 methylation is often disrupted when subunits of Set1-COMPASS are mutated (*15*).

The regulation of H3K4 methylation involves cross-talk with other modifications on histone tails. A notable example is the ubiquitination of histone H2B at K123 in yeast (K120 in mammals) by Rad6-Bre1: Loss of function of Rad6-Bre1 substantially decreases the H3K4me3 and H3K4me2 levels in yeast (*16*, *17*). The normal patterns of H3K4 methylation are also shaped by several factors involved in H2B ubiquitination, including Bur1/Bur2, the RNA Pol II–associated factor (PAF) complex, and the Ccr4-Not complex (*14*, *18*, *19*). H3K4 methylation is also influenced by the acetylation of H3 at K14 by the SAGA and/or NuA3 histone acetyltransferases (HATs) (*20*, *21*). H3K4 methylation patterns are also affected by methylation of the adjacent arginine residue H3R2 (*22*, *23*). Thus, the complex interactions that regulate H3K4 methylation are understood to some extent. However, it remains largely unclear whether (and which) posttranslational modifications of the Set1-COMPASS complex itself control its functions.

N-terminal acetylation is the acetylation of the first amino acid of proteins and is the most common posttranslational modification (*24*, *25*). It is mediated by N-terminal acetyltransferases (NATs), which transfer an acetyl group from acetyl–coenzyme A to the Nα terminus of the protein substrate (*26*, *27*). N-terminal acetylation affects protein-protein interactions, stability, and/or

[1]Department of Life Science and Multitasking Macrophage Research Center, Ewha Womans University, Seoul 03760, Republic of Korea. [2]Department of Molecular Bioscience, College of Biomedical Science, Kangwon National University, Chuncheon 24341, Republic of Korea. [3]Multidimensional Genomics Research Center, Kangwon National University, Chuncheon, Republic of Korea. [4]Korea Bioinformation Center, Korea Research Institute of Bioscience and Biotechnology, Daejeon 34141, Republic of Korea. [5]Proteomics Core Facility, Biomedical Research Institute, Seoul National University Hospital, Seoul 03082, Republic of Korea. [6]Department of Transdisciplinary Medicine, Seoul National University Hospital, Seoul 03082, Republic of Korea. [7]Department of Medicine, Seoul National University College of Medicine, Seoul 03082, Republic of Korea.
*Corresponding author. Email: tskim@ewha.ac.kr (T.K.); jungshinlee@kangwon.ac.kr (J.-S.L.)
†These authors contributed equally to this work.

localization, thereby shaping protein functions (*28*–*30*) and playing key roles in multiple cellular processes (*24*, *25*). Five distinct NATs (NatA to NatE) with different specificities have been identified in yeast (*30*). Each consists of a catalytic subunit: In yeast, examples are Ard1 in NatA and Nat3 in NatB (*25*). The NATs also contain one or several adaptor subunits: Examples are Nat1 and Nat5 in NatA. NatA deficiency affects histone modifications: For example, loss of the catalytic subunit of NatA (*NAA10*, which is known as Ard1 in yeast) substantially reduces global histone acetylation in *Drosophila melanogaster* (*31*). Moreover, deletion of Ard1 or Nat1 impairs H2B ubiquitination. Notably, this in turn may reduce H3K4 trimethylation by Set1-COMPASS and H3K79 trimethylation by the histone methyltransferase Dot1 (*32*–*34*). However, the mechanisms by which NatA deficiency shapes H2B ubiquitination, and H3K4 and K79 methylation remain unclear.

These observations together led us to speculate that N-acetylation of chromatin-modifying enzymes by NATs can directly shape their functions. Many such enzymes, including Set1-COMPASS, HATs, and histone deacetylases (HDACs), undergo N-terminal acetylation by NATs (*35*). Thus, we hypothesized that NatA may directly regulate H3K4 methylation by acetylating the N terminus of one or more of the proteins in the Set1-COMPASS complex.

Here, we show that N-terminal acetylation of Set1-COMPASS subunits by NatA and NatB finely tunes H3K4 methylation patterns. First, chromatin immunoprecipitation sequencing (ChIP-seq) reveals that loss of Ard1 led to noncanonical H3K4 methylation patterns, namely, substantial reduction in H3K4me3 at promoters and shifting of the H3K4me2 peak from 5′ transcribed regions to the promoters. Second, biochemical investigations showed that N-terminal acetylation of Shg1, Spp1, and Swd2 depends on NatA and that blocking this activity impaired H3K4 methylation patterns. Specifically, preventing NatA-mediated N-terminal acetylation of Shg1 by mutating the first amino acid [alanine to proline (A2P)] greatly decreased global and gene-specific H3K4 methylation levels. This change did not involve altered H2B ubiquitination. Last, we found that Nat3, the catalytic subunit of NatB, and its potential target, Swd1, which is part of WRAD, were needed for maintaining normal levels of H3K4 methylation. On the basis of these findings, we propose that direct N-terminal acetylation of the Set1-COMPASS complex is an additional mechanism that modulates H3K4 methylation patterns.

RESULTS

Canonical H3K4 methylation patterns depend on the NatA complex

H3K4 methylation by Set1-COMPASS can be regulated by multiple factors. One is Rad6-Bre1, which ubiquitinates H2B at K123. Specifically, loss of function in Rad6/Bre1 reduces H3K4me3 and H3K4me2 levels (*16*, *17*). Another regulator of H3K4 methylation is NatA. Deficiency in its Ard1 or Nat1 component also reduces H3K4me3 levels, but the mechanisms involved are unclear. Because loss of Ard1 or Nat1 also decreases H2B ubiquitination (*34*), it is possible that the lower H3K4me3 levels in mutants for Ard1 or Nat1 are secondary to impaired Rad6-Bre1–mediated H2B ubiquitination. However, it is also possible that NatA directly affects H3K4 methylation patterns by N-terminal acetylation of Set1-COMPASS proteins.

To determine whether NatA can directly regulate H3K4 methylation, we created mutants for Ard1, Nat1, and Nat5: All of these proteins are NatA complex components. Western blot analyses confirmed that deleting *ARD1* or *NAT1*, but not *NAT5*, reduced global H2B ubiquitination. These mutations also greatly reduced global H3K79me3 levels, which are generated by the histone methyltransferase Dot1. In addition, H3K4me3, H3K4me2 and H3K4me1 levels were also decreased in these mutants (Fig. 1A). We next determined gene-specific patterns of H3K4 methylation by chromatin immunoprecipitation (ChIP) assays using antibodies against H3K4me2 or H3K4me3. Levels of these modifications were normalized to total histone H3 levels. As previously reported, H3K4me3 and H3K4me2 were highly enriched at promoters and 5′ regions, respectively, of two highly expressed genes, *PYK1* and *YEF3* in wild-type cells (*36*) (Fig. 1B and fig. S1A). Both H3K4me3 and H3K4me2 peaked at promoters at *PMA1* gene but were high at 5′ regions and 3′ regions of *RPS13*, respectively (fig. S1, B and C). Loss of Ard1 or Nat1, but not Nat5, altered the H3K4 methylation patterns in all four genes. In *PYK1* and *YEF3*, the high H3K4me3 levels at the promoter were substantially reduced, and the H3K4me2 peak shifted from the 5′ region to the promoter (Fig. 1B and fig. S1A). Thus, the H3K4 methylation patterns changed from canonical to noncanonical. In *PMA1*, the H3K4me3 and H3K4me2 peaks at the promoter both dropped, and the low levels of both in the gene remained low. In *RPS13*, high H3K4me3 levels were maintained in the promoter and 5′ regions, but the H3K4me3 levels in the 3′ region dropped substantially. Moreover, while the higher H3K4me2 levels in the *RPS13* 3′ regions were maintained, loss of Ard1 or Nat1 strongly elevated H3K4me2 levels in the promoter and 5′ regions (fig. S1, B and C). Thus, mutants for NatA markedly changed the patterns of H3K4 methylation in individual genes. We then asked whether the methylation pattern changes induced by NatA deficiency were the same as those generated by deleting Rad6 or Bre1: This would be the case if NatA shapes H3K4me3 levels via Rad6-Bre1, which then correctly ubiquinates H2B, which in turn alters H3K4me3 levels. However, the H3K4 methylation patterns generated on *PYK1* and *YEF3* by the *ARD1* and *NAT1* deletions were different from those produced by deleting *RAD6* or *BRE1*: The latter deletions caused a profound loss of both H3K4me3 and H3K4me2 throughout the promoter and gene bodies (fig. S1, D and E).

To determine whether the changed H3K4 methylation patterns in the NatA mutants reflected defective Set1-COMPASS cross-linking, we examined the effect of *ard1*Δ on Set1 occupancy. Thus, strains that expressed Set1 linked to 3X hemagglutinin (HA) or tandem affinity purification (TAP) were subjected to ChIP-seq. Although genome-wide occupancy of Set1 was only slightly reduced in *ARD1*-deleting cells, its localization remained unchanged (Fig. 1, C and D, and fig. S1, F and G). To test whether *ard1*Δ affects the assembly or the levels of the individual subunits of the Set1-COMPASS complex, we subjected TAP-purified Set1-COMPASS complexes to mass-spectrometry (MS) analysis and silver staining. However, *ard1*Δ did not change the composition of Set1-COMPASS nor the levels of its individual subunits (Fig. 1, E and F). Note that while Shg1 levels seemed slightly reduced in the MS analysis, coimmunoprecipitation analyses did not confirm this reduction (Fig. 1G). Thus, the severe H3K4 methylation defects in NatA mutants are unlikely to be due to altered Set1-COMPASS chromatin binding, assembly, or individual subunit levels.

To further elucidate the role of NatA in H3K4 methylation patterns, we used ChIP-seq to determine the genome-wide H3K4me3 and H3K4me2 patterns in wild-type and *ard1*Δ strains. *Schizosaccharomyces*

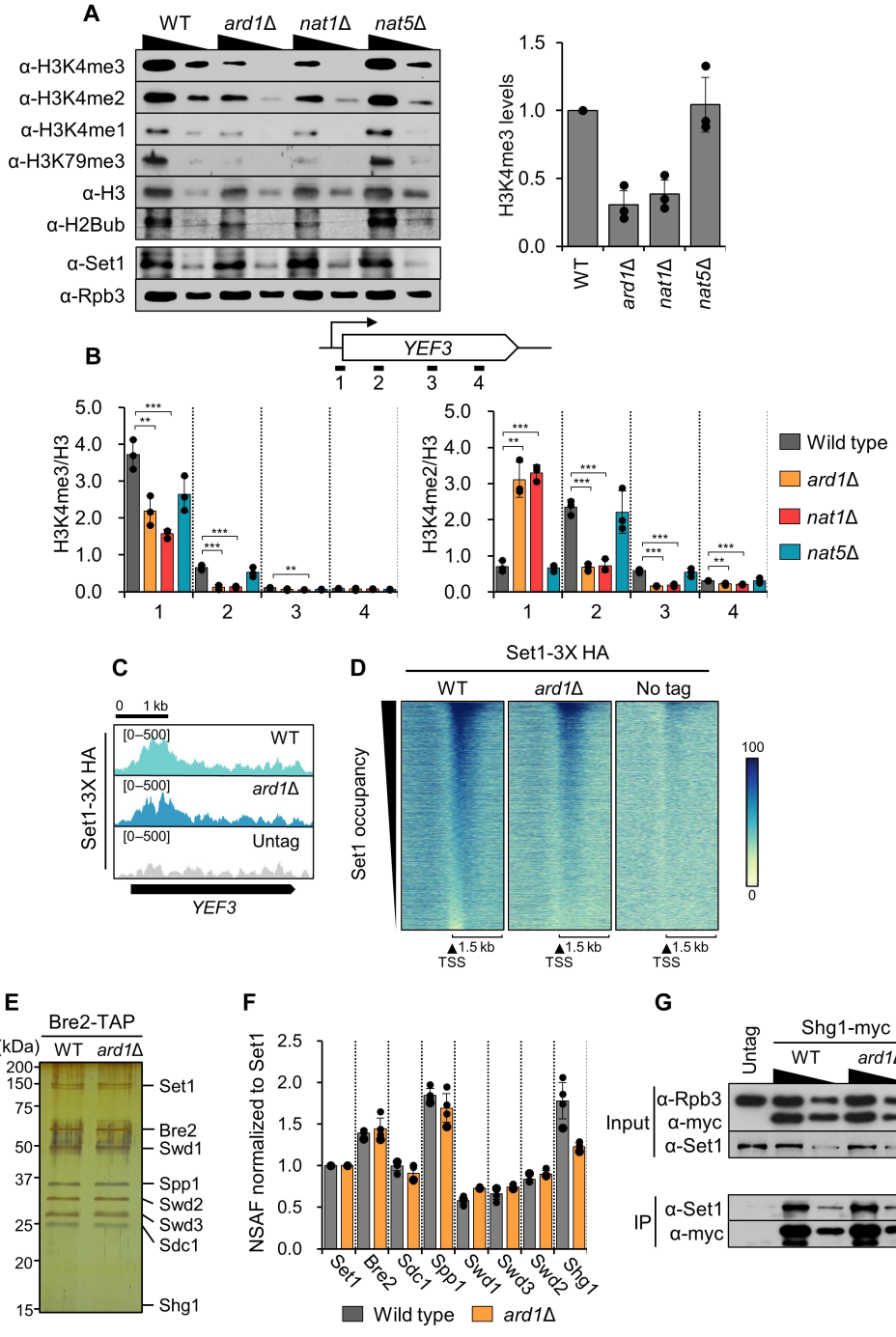

Fig. 1. Mutants that lack NatA complex display altered H3K4 methylation patterns. (**A**) Whole-cell extracts from the indicated strains were subjected to Western blot analysis of the indicated histone modifications (left). Histone H3 and Rpb3 were used as loading controls. H3K4me3 signal intensity from each immunoblot was quantitated using ImageJ. Error bars show the SD calculated from three biological replicates. Values from wild type (WT) were set to 1.0 (right). (**B**) Cross-linked chromatin from the strains was precipitated with the indicated antibodies. The precipitated DNA was subjected to polymerase chain reaction (PCR) analysis on *YEF3* using the primer pairs indicated in the upper panels. The signals for H3K4me3 and H3K4me2 were normalized to the H3 signal, and the ratios were graphed. Error bars show the SD calculated from three biological replicates, each with three technical replicates. $*P < 0.05$, $**P < 0.01$, and $***P < 0.001$ (two-tailed unpaired Student's *t* tests). (**C**) ChIP-seq tracks of Set1 occupancy on *YEF3* in WT and *ard1*Δ strains. (**D**) Heatmaps of ChIP-seq signals for Set1 occupancy in the indicated strains. The data are from two independent experiments. The *y* axis indicates each gene, and the *x* axis indicates relative position to the TSS. All genes are sorted in descending order of Set1 signals in WT. The right panel indicates the scale of RPM (reads per million) values. (**E**) TAP-purified Set1-COMPASS complexes from the indicated strains were visualized by silver staining. (**F**) Purified Set1-COMPASS from the indicated strains were subjected to Multidimensional Protein Identification Technology (MudPIT). Spectral counts normalized against protein length (NSAF) were determined for purified Set1-COMPASS. (**G**) Whole-cell extracts from the indicated strains were immunoprecipitated with α-myc antibody or protein G beads, and the precipitates were resolved by SDS–polyacrylamide gel electrophoresis (SDS-PAGE) followed by immunoblot analysis.

pombe spike-in control normalization was included to ensure that the H3K4 methylation pattern changes were accurate. We first examined the changes induced by deletion of *ARD1* on the *YEF3* gene. The same changes shown in Fig. 1B were observed: Loss of Ard1 markedly reduced the enrichment of H3K4me3 in the promoter and shifted the H3K4me2 peak from the 5′ transcribed region to the promoter. By contrast, *ARD1* deletion had no effect on histone H3 ChIP-seq patterns (Fig. 2A). We then examined the total yeast genes ($n = 6020$). A heatmap depicting the 3000–base pair (bp) window around the TSSs of these yeast genes showed that in wild-type cells, the H3K4me3 levels were highest in the promoters and H3K4me2 peaked in the 5′ transcribed regions. However, there was also a small portion of genes in the

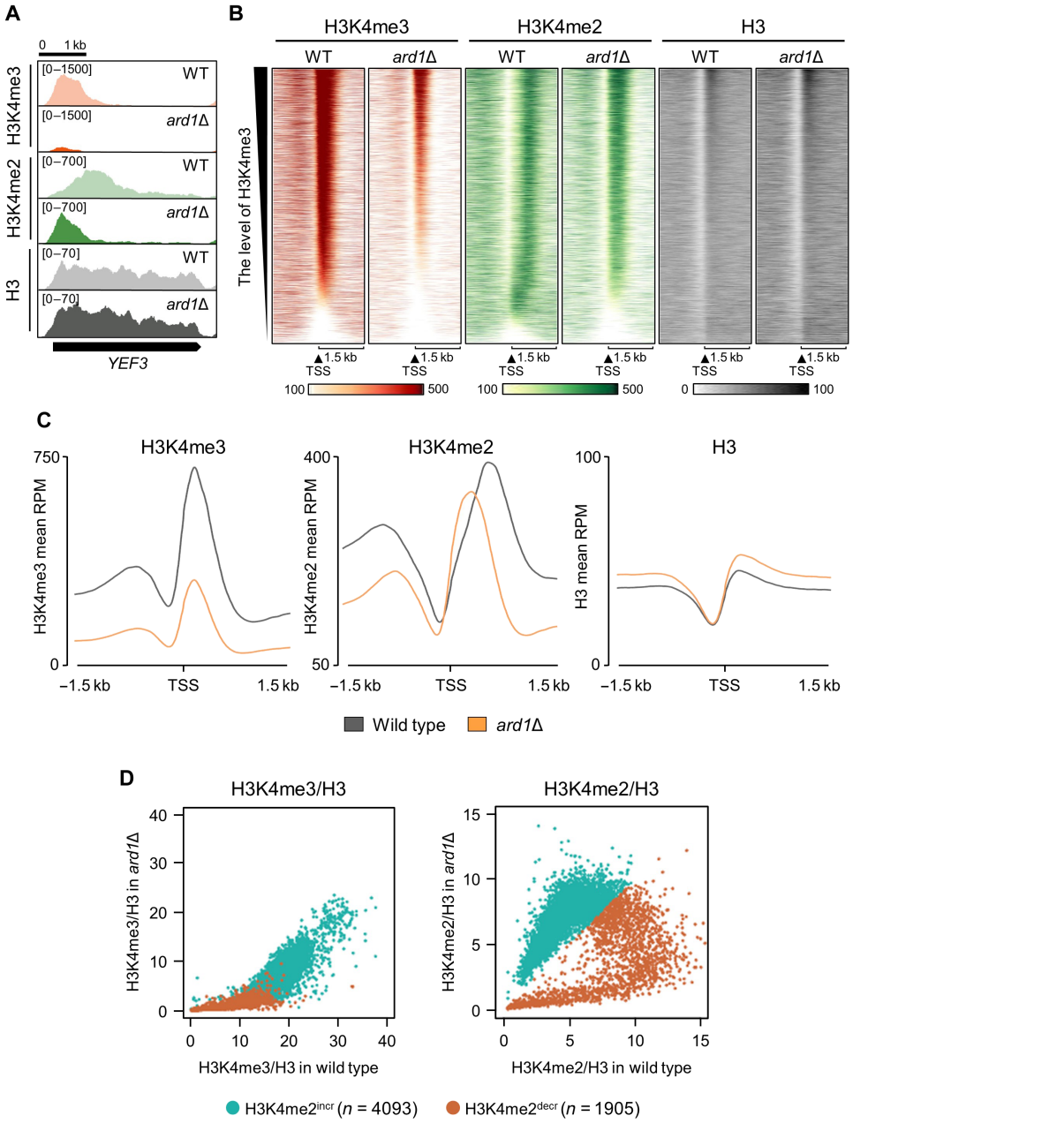

Fig. 2. NatA is required for canonical H3K4 methylation patterns. (**A**) ChIP-seq tracks of the H3K4me3 and H3K4me2 signals and H3 occupancy at *YEF3* in the *ard1*Δ and WT strains. (**B**) Heatmaps of ChIP-seq signals for H3K4me3 (red), H3K4me2 (green), and histone H3 (gray) in WT and *ard1*Δ strains. The data are from two independent experiments. The *y* axis indicates each gene, and the *x* axis indicates relative position to the TSS. All genes are sorted in descending order of H3K4me3 signals in WT. The lower panels indicate the scale of RPM values (100 to 500 for H3K4me3 and H3K4me2; 0 to 100 for H3). (**C**) Average plots of ChIP-seq signals for H3K4me3, H3K4me2, and H3 in WT (gray) and *ard1*Δ (orange) strains. The signals were plotted over a 3-kb window that centered on the TSS. The *y* axis indicates the average RPM. (**D**) Scatter plots of H3K4me3 and H3K4me2 at the promoter of each gene in the total genome of WT and *ard1*Δ strains. The ChIP-seq signals of H3K4me3 (left) and H3K4me2 (right) were normalized by the H3 signal in the promoter region (from −100 to +300 bp). The signals from WT and *ard1*Δ strains were plotted on the *x* axis and *y* axis, respectively. The total genes were subdivided into two groups based on whether the Ard1 deletion caused the H3K4me2 levels at the promoter region to increase (H3K4me2^{incr} group; $n = 4093$; cyan) or decrease (H3K4me2^{decr}; $n = 1905$; brown).

genome that exhibited noncanonical H3K4 methylation patterns, namely, an H3K4me2 peak at the promoter and no H3K4me3. Deleting *ARD1* changed all three patterns: The canonical H3K4me3 peak in the promoters was greatly reduced, the canonical H3K4me2 peak shifted from the 5′ ends to the promoters (Fig. 2, B and C), and the noncanonical genes lost their H3K4me2 marks in the promoter.

Similar observations were made when we used K-mean clustering to divide the total yeast genes into two groups according to whether loss of Ard1 caused the H3K4me2 levels in the promoter regions (−100 to +300 bp) to rise (H3K4me2^{incr} group, cyan) or fall (H3K4me2^{decr} group, brown). Figure 2D shows scatterplots of the H3K4me3/H3 and H3K4me2/H3 levels in the promoters of the two groups in wild-type and *ard1*Δ strains. Approximately 68% of the genes were in the H3K4me2^{incr} group (n = 4093). Heatmaps of the 3000-bp window around the TSSs of the two groups in fig. S2 (A and B) showed that in wild-type cells, the H3K4me2^{incr} genes had high H3K4me3 levels in the promoters and high H3K4me2 levels in the 5′ transcribed regions. When *ARD1* was deleted, the H3K4me3 levels dropped substantially, and the H3K4me2 peak shifted to the promoter regions. By contrast, the H3K4me2^{decr} genes (n = 1905) showed enrichment of both H3K4me3 and H3K4me2 in the promoters in wild-type cells, and this was reduced in mutants for Ard1 (fig. S2, A and B). These findings indicate that the NatA complex is required not only for normal levels of H3K4 methylation but also for the canonical patterns of this modification.

NatA and NatB mediate N-terminal acetylation of Set1-COMPASS

Because NatA is an N-terminal acetyltransferase and deleting its catalytic subunit greatly disturbed H3K4 methylation patterns (Figs. 1 and 2), it seems likely that it regulates H3K4 methylation patterns by acetylating the first residue of one or more proteins in Set1-COMPASS complex. This notion is the fact that NatA acetylates many chromatin modifiers (*35*). However, the posttranslational modifications of the Set1-COMPASS that affect its function remain unknown (*37*–*39*).

To test whether NatA could shape H3K4 methylation patterns by N-terminal acetylation of Set1-COMPASS, we first analyzed the amino acid sequences of all Set1-COMPASS proteins to determine whether they bore NatA-target consensus sequences. Set1 and all non-WRAD proteins of COMPASS, namely, Spp1, Swd2, and Shg1, were potential NatA targets. This is supported by Soares *et al.* (*15*), who showed that deleting *SPP1* strongly reduced H3K4me3 levels and shifted the H3K4me2 peak in the 5′ regions to the promoters. Because budding yeast also expresses four other NATs (NatB to NatE) with distinct specificities (*30*), we also examined whether any of the Set1-COMPASS proteins were targets for NatB and NatC. The WRAD proteins Swd1 and Sdc1 were potential NatB targets, while the WRAD protein Swd3 was a possible NatC target (Fig. 3A). Thus, seven of the eight Set1-COMPASS proteins could potentially undergo N-terminal acetylation.

To determine the N-terminal acetylation status of Set1-COMPASS subunits in the wild type, we subjected TAP-purified Set1 complexes to liquid chromatography–tandem mass spectrometry (LC-MS/MS) analysis. N-terminal acetylation was only observed on four subunits: Shg1, Spp1, Swd2, and Swd1. Only partial N-terminal acetylation was observed on Shg1 (75%), Spp1 (80%), and Swd2 (57%). By contrast, the WRAD protein Swd1 exhibited 100% N-terminal acetylation. In addition, N-terminal acetylation of Set1 and the remaining

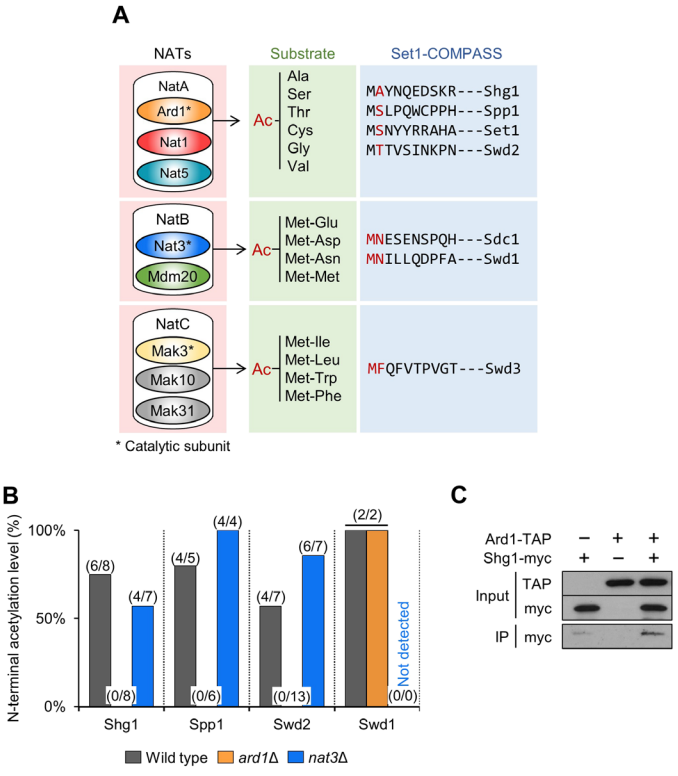

Fig. 3. NatA acetylates the N terminus of Shg1. (**A**) The target sequences of NatA, NatB, and NatC and their potential targets of Set1-COMPASS subunits. (**B**) N-terminal acetylation levels of Set1-COMPASS subunits. Purified Set1-COMPASS complexes from two-step TAP purification using Bre2-TAP (WT, *ard1*Δ, or *nat3*Δ) were analyzed by LC-MS/MS. The number of acetylated N-terminal peptides of each component was divided by the total N-terminal peptide numbers. The numbers in parentheses represent the ration between acetylated N-terminal peptide number and total N-terminal peptide number. (**C**) NatA interacts physically with Shg1. Whole-cell extracts from the indicated strains were immunoprecipitated with IgG Sepharose. The bead-bound complexes were treated with TEV protease and the eluates were resolved by SDS-PAGE followed by immunoblot analysis.

WRAD proteins Bre2, Swd3, and Sdc1 was not detected. Given that the N-acetylated proteins were targets of NatA or NatB (Fig. 3A), we repeated the LC-MS/MS analysis with the *ard1*Δ and *nat3*Δ strain: The latter lacks the catalytic subunit of NatB. Loss of Ard1 resulted in the complete absence of N-terminal acetylation on the putative NatA targets Shg1, Spp1, and Swd2; the putative NatB target Swd1 remained fully N-acetylated (Fig. 3B). Similarly, a previous study showed that 56% of Shg1 N termini were acetylated in wild-type cells, but this modification was completely absent in *ard1*Δ mutants (*35*). With regard to the *nat3*Δ strain, its N-terminal-acetylation patterns were similar to those of wild-type cells (Fig. 3B). Thus, both amino acid sequence analysis and LC-MS/MS data strongly suggest that N-terminal acetylation of Shg1, Spp1, and Swd2 is dependent on NatA, while Swd1 is a potential target of NatB.

Because N-terminal acetylation of multiple subunits of the Set1-COMPASS requires NatA, we next asked whether NatA and the complex associate physically. Coimmunoprecipitation assays with cells expressing both Ard1-TAP and Shg1-myc suggested that NatA

physically interacts with the Set1-COMPASS and likely mediates N-terminal acetylation of at least three subunits: Shg1, Spp1, and Swd2 (Fig. 3C).

N-terminal acetylation of Shg1 shapes the ability of the Set1-COMPASS to catalyze H3K4 methylation

The function of Shg1 remains unclear: Kim *et al.* (*12*) have shown that deleting Shg1 does not affect Set1-COMPASS assembly or the H3K4 methyltransferase activity of the in vitro reconstituted complex. Moreover, deletion of *SHG1* had no effect on the protein stability of Set1 and global levels of H3K4 methylation (*40*). Consequently, Shg1 has been thought to be nonessential for Set1-COMPASS activity. However, a previous study showed that transient nuclear depletion of Shg1 by an anchor-away system resulted in the substantial reduction of global H3K4 methylation (*41*). Although this could be due to depletion of the whole complex, it nonetheless suggested that Shg1 might play an as-yet unknown role in regulating H3K4 methylation.

To explore this potential function of Shg1, we first used Western blot analysis to assess the effect of deleting *SHG1* on global H3K4 methylation levels. H3K4me3 and H3K4me2 levels were not changed in *shg1*Δ as previously reported (*40*, *42*) (Fig. 4A). In addition, the patterns of these modifications on *PYK1* and *YEF3* genes were compatible to wild-type cells (fig. S3). Thus, deleting *SHG1* on its own indeed has no marked effect on H3K4 methylation. Because Soares *et al.* have shown that *spp1*Δ strains had a marked effect on H3K4 methylation (*15*) that was similar to the effect of *ARD1* or *NAT1* deletion (Figs. 1 and 2), we then asked whether loss of Shg1 together with Spp1 further altered H3K4 methylation patterns. We first showed that as expected (*15*), *SPP1* deletion substantially decreased global H3K4me3 levels, while H3K4me2 levels were slightly reduced. The effect on H3K4me3 levels was not due to changes in H2B ubiquitination, which was unaltered by *SPP1* deletion. The double *shg1*Δ*spp1*Δ knockout showed almost complete loss of H3K4me3, and H3K4me2 was also decreased relative to the levels in *spp1*Δ (Fig. 4A). ChIP analyses of the *YEF3* and *PYK1* genes then showed that *SPP1* deletion on its own decreased H3K4me3 levels and shifted the H3K4me2 peak from the 5′ regions to the promoter. Deletion of both *SPP1* and *SHG1* resulted in complete loss of H3K4me3 and strongly reduced H3K4me2 levels (fig. S3). Similarly, ChIP-seq analysis of H3K4me3 and H3K4me2 in the wild-type, *shg1*Δ, *spp1*Δ, and *shg1*Δ*spp1*Δ strains showed that for the *YEF3* gene, *SPP1* deletion alone markedly reduced H3K4me3 levels and caused the H3K4me2 peak to shift sharply to the promoter. When *SHG1* was deleted on its own, there was a slight shift of the H3K4me2 peak to the promoter but no change in H3K4me3 pattern. However, when the *SPP1* and *SHG1* deletions were combined, the strong promoter-ward shift of H3K4me2 was seen again, but this time, the H3K4me2 levels were much lower. Moreover, the H3K4me3 levels were abolished in the double mutant (Fig. 4B). Analysis of the ChIP-seq data confirmed these findings for the whole genome (Fig. 4, C and D). These results strongly suggest that Shg1 plays a minor but important role in the regulation of H3K4 methylation.

To test whether N-terminal acetylation of Shg1 shaped H3K4 methylation, we replaced the N-terminal residue of Shg1 (alanine) with proline, a residue that is usually not acetylated (*43*, *44*). This was repeated with Spp1 and Set1 (in both, serine was the target residue). Western blot analysis of the resulting mutant cells was then conducted to determine the global H3K4 methylation patterns. The Ser-to-Pro (S2P) mutations in Spp1 and Set1 did not alter H3K4 methylation levels (Fig. 5A). Moreover, although our LC-MS/MS and coimmunoprecipitation analyses (Fig. 3, B and C) and Van Damme *et al.* (*35*) showed that Shg1 is a direct target of NatA, the Ala-to-Pro (A2P) mutation in Shg1 also had no detectable effect on H3K4 methylation (Fig. 5A). This was also observed when the *shg1*A2P mutation was combined with the *set1*S2P or *spp1*S2P mutations (fig. S4A) and when all three mutations were present (Fig. 5B).

We then asked whether the A2P mutation in Shg1 affected H3K4 methylation if *SPP1* had been deleted, because Shg1 only exerted an effect on H3K4 methylation when it was deleted along with *SPP1* (Fig. 4). The *shg1*A2P*spp1*Δ cells displayed lower global H3K4me3 and H3K4me2 levels than the *spp1*Δ cells (Fig. 5C). By contrast, combining the *set1*S2P mutation with *SPP1* deletion had no effect on H3K4 methylation levels (Fig. 5D). The effect seen in the *shg1*A2P *spp1*Δ cells was also observed when the N-terminal residue of Shg1 was replaced with cysteine (A2C), another residue that is unlikely to be acetylated, and *SPP1* was deleted (fig. S4B).

We then examined whether the physical interaction between Shg1 and Ard1, which we had observed with coimmunoprecipitation analyses (Fig. 3C), was affected by the *shg1*A2P mutation. However, coimmunoprecipitation analyses with *shg1*A2P cells showed the mutation did not affect the binding of Shg1 to Ard1 (fig. S4C). While *SPP1* deletion did reduce Set1 levels (fig. S4D), this could not explain the effect of adding the *shg1*A2P mutation to the *spp1*Δ mutation: The Set1 levels in the double *shg1*A2P*spp1*Δ mutant (and the *shg1*Δ*spp1*Δ mutant) were comparable to those in *spp1*Δ alone (fig. S4D). These findings together suggest that N-terminal acetylation of Shg1 by NatA is important for fine-tuning H3K4 methylation.

NatB also shapes H3K4 methylation

Both amino acid sequence analysis and the LC-MS/MS data suggested that N-terminal acetylation of Swd1 is likely dependent on NatB (Fig. 3, A and B). This suggests that NatB may also regulate H3K4 methylation by N-terminal acetylation of Set1-COMPASS.

To test this, we deleted Nat3, the catalytic subunit of NatB, and assessed H3K4 methylation levels with Western blotting. No detectable changes in global H3K4 methylation levels were observed (Fig. 6A). However, when we deleted both *SPP1* and *NAT3*, both H3K4me3 and H3K4me2 were substantially reduced (Fig. 6A). This is similar to what we observed for Shg1 above, namely, the effect of its deletion/A2P mutation on H3K4 methylation only emerged when *SPP1* was deleted (Fig. 4A). Moreover, deleting both *SHG1* and *NAT3* had the same effect: H3K4me3 and H3K4me2 levels dropped (fig. S5A). In addition, unlike when ARD1 was deleted, the loss of Nat3 did not affect H2B ubiquitination (Fig. 6A and fig. S5A). To further explore the role of NatB in H3K4 methylation, we conducted ChIP assays. Consistent with the Western blot analyses, *NAT3* deletion had no detectable effect on the H3K4me3 and H3K4me2 patterns in *PYK1* or *YEF3* unless *SPP1* was also deleted: In that case, the H3K4me3 levels vanished and the H3K4me2 peak shifted from the 5′ region to the promoter (Fig. 6B and fig. S5B). Deletion of *NAT3* did not affect the composition of Set1-COMPASS (fig. S5C).

We next assessed the effect of blocking N-terminal acetylation on Swd1 and Sdc1, another potential target of NatB, on H3K4 methylation. Thus, the target residue of Swd1 and Sdc1 (both asparagine) was replaced with proline (N2P). The N2P mutation in Swd1 but not in Sdc1 slightly reduced H3K4me3. Notably, when *SPP1* was deleted, the *swd1*N2P mutation substantially reduced the H3K4me3 and H3K4me2 levels. However, this was not observed for the *sdc1*N2P

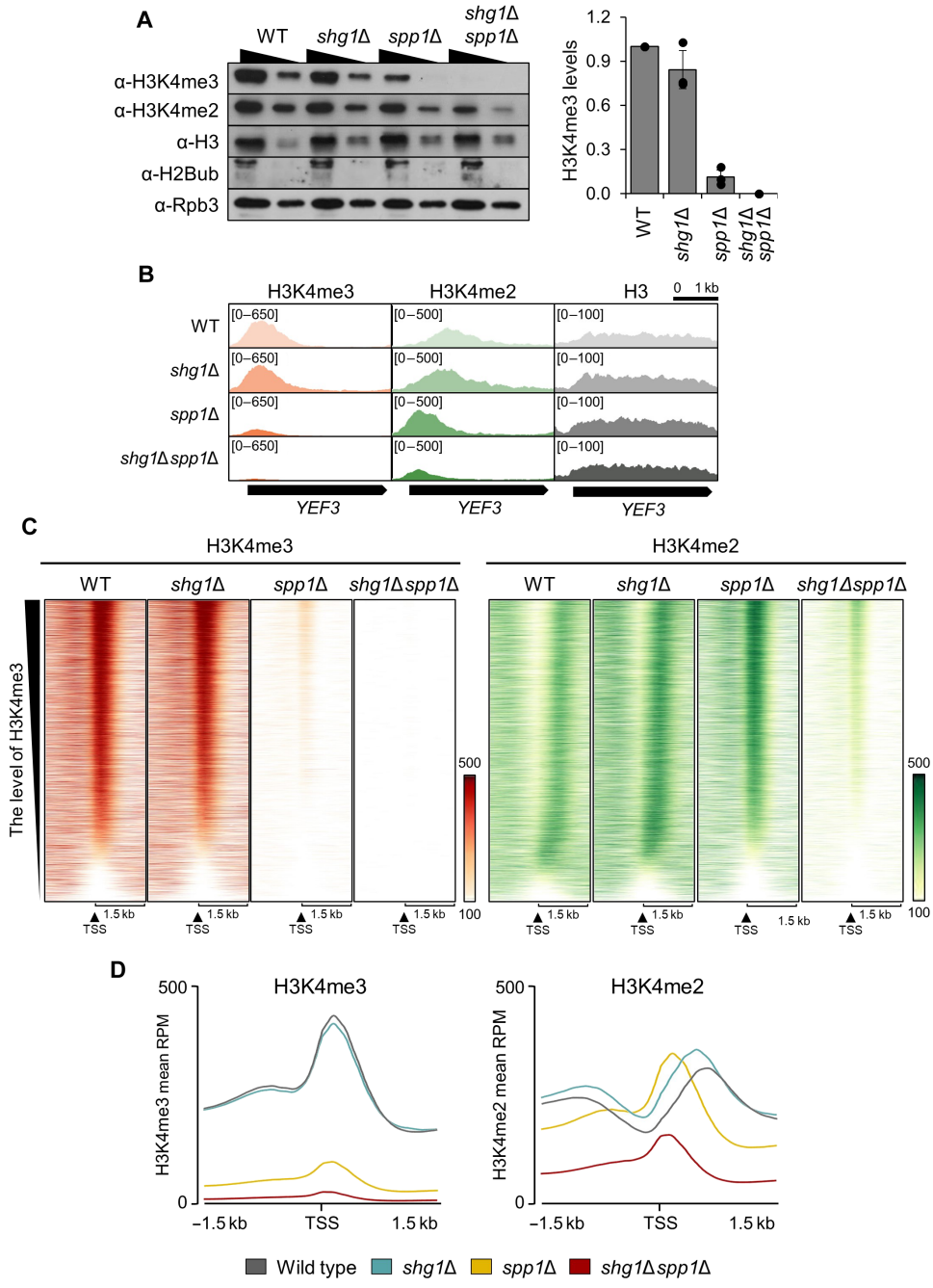

Fig. 4. Shg1 is required for optimal H3K4 methylation. (**A**) Loss of Shg1 reduces H3K4me3 and H3K4me2 in *SPP1*-deleting cells. Whole-cell extracts from WT, *shg1*Δ, *spp1*Δ, and *shg1*Δ*spp1*Δ were subjected to Western blot analysis using indicated antibodies (left). Histone H3 and Rpb3 were used as loading controls. H3K4me3 signal intensity from each immunoblot was quantitated using ImageJ. Error bars show the SD calculated from three biological replicates. Values from WT were normalized to 1.0 (right). (**B**) ChIP-seq tracks for the signals of H3K4me3, H3K4me2, and H3 on *YEF3* in the indicated strains. (**C**) Heatmaps of ChIP-seq signals for H3K4me3 and H3K4me2 in the indicated strains were generated from two independent experiments. All genes ($n = 6020$) are sorted in descending order of the H3K4me3 signal in WT, as described in Fig. 2B. (**D**) Average plots of ChIP-seq for H3K4me3 and H3K4me2 in the indicated strains.

*spp1*Δ cells (Fig. 6, C and D, and fig. S5, D and E). Again, H2B ubiquitination was unaffected in the double *swd1*N2P *spp1*Δ mutant (Fig. 6C). These observations together suggest that H3K4 methylation patterns are regulated not only by NatA-mediated N-terminal acetylation of Shg1 in Set1-COMPASS but also by NatB-mediated N-terminal acetylation of Swd1.

DISCUSSION

H3K4 methylation is highly conserved from yeast to humans and is regulated by multiple factors. This study shows that posttranslational modifications of the Set1-COMPASS also regulate H3K4 methylation. Specifically, N-terminal acetylation of the Set1-COMPASS subunits can fine-tune H3K4 methylation patterns. This was revealed

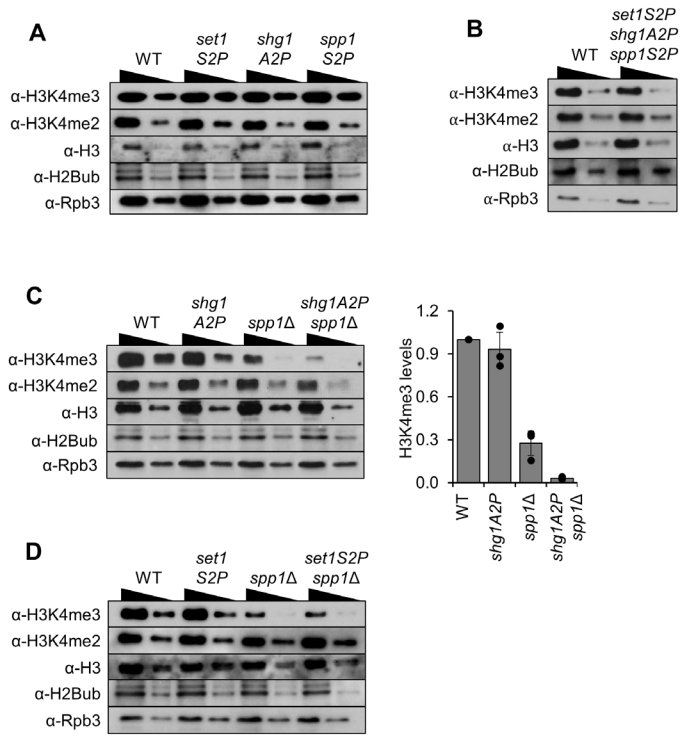

Fig. 5. N-terminal acetylation of Shg1 is required for H3K4 methylation. The N-terminal acetylation site of Shg1 (alanine) was replaced with proline (A2P), which is rarely acetylated. This was repeated for the serine N-terminal acetylation site of Set1 and Spp1 (S2P). All experiments involved Western blot analysis of whole-cell extracts to detect the levels of the indicated histone modifications. Histone H3 and Rpb3 were used as loading controls. (**A**) None of the N-terminal acetylation site mutations affected H3K4 methylation. (**B**) All three mutations together did not affect H3K4 methylation. (**C**) A2P mutation of *SHG1* reduced H3K4 methylation in *SPP1*-deleting cells. H3K4me3 signal intensity from each immunoblot (left) was quantitated using ImageJ. Error bars show the SD calculated from three biological replicates. Values from WT were normalized to 1.0 (right). (**D**) Combining the S2P mutation of Set1 with *SPP1* deletion had no effect on H3K4 methylation.

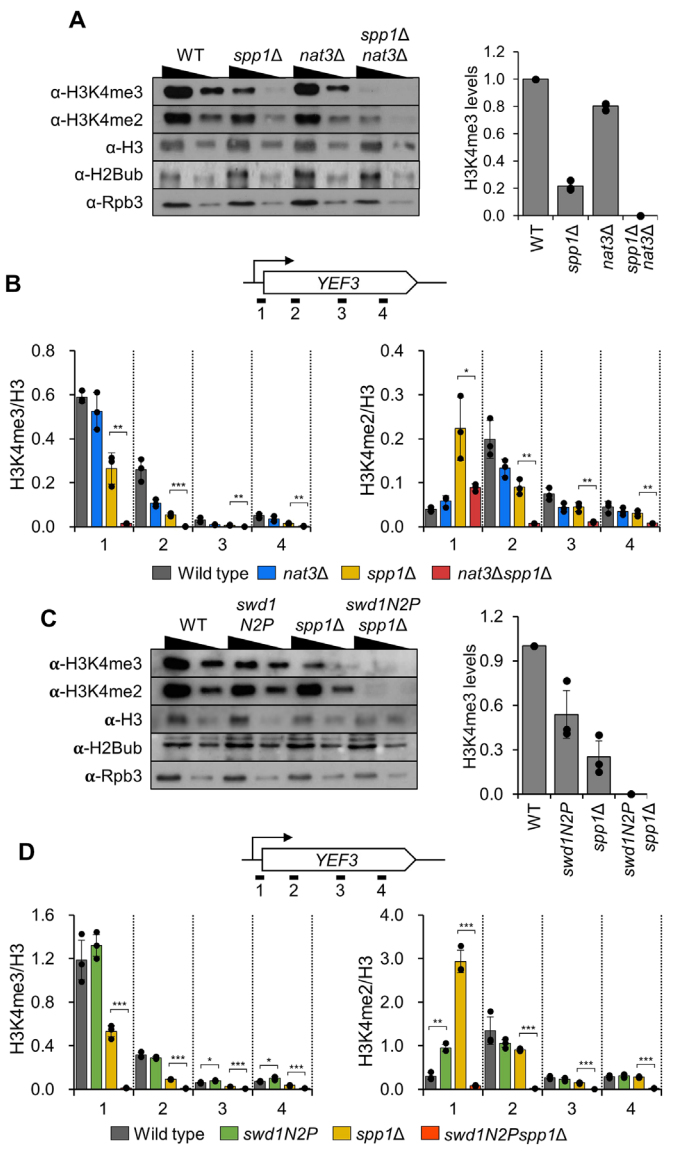

Fig. 6. NatB is also required for optimal H3K4 methylation. (**A**) Loss of Nat3 affects H3K4 methylation in *SPP1*-deleting cells. Western blot analyses were done as described in Fig. 1A. H3K4me3 signal intensity from each immunoblot (left) was quantitated using ImageJ. Error bars show the SD calculated from three biological replicates. Values from WT were normalized to 1.0 (right). (**B**) Loss of Nat3 reduces H3K4 methylation in *SPP1*-deleting cells. Cross-linked chromatin from the indicated strains was precipitated with anti-H3K4me3, anti-H3K4me2, or anti-H3. The precipitated DNA was subjected to PCR analysis on the *YEF3* gene using the primer pairs indicated in the upper panels. The signals for H3K4me3 and H3K4me2 were quantified and normalized to the H3 signal, and the ratios were graphed. A non-transcribed region near the telomere of chromosome VI was used for an internal control. Error bars show the SD calculated from three biological replicates, each with three technical replicates. $*P < 0.05$, $**P < 0.01$, and $***P < 0.001$ (two-tailed unpaired Student's *t* tests). (**C** and **D**) N2P mutation of Swd1 reduces H3K4 methylation in *SPP1*-deleting cells. (C) Whole-cell extracts from the indicated strains were subjected to Western blot analysis. H3K4me3 signal intensity from each immunoblot (left) was quantitated using ImageJ (right). Error bars show the SD calculated from three biological replicates. Values from WT were normalized to 1.0 (right). (D) ChIP analysis was done as described in (B). Error bars show the SD calculated from three biological replicates, each with three technical replicates. $*P < 0.05$, $**P < 0.01$, and $***P < 0.001$ (two-tailed unpaired Student's *t* tests).

by several observations. First, loss of NatA resulted in a substantial reduction of H3K4me3 and a shift of H3K4me2 peak from 5′ transcribed regions to promoters even though the assembly and the levels of individual subunits of Set1-COMPASS remained unchanged (Figs. 1 and 2). Second, NatA interacted directly with Set1-COMPASS and mediated N-terminal acetylation of Shg1, Spp1, and Swd2 subunits (Fig. 3). Moreover, deleting *SHG1* or blocking its N-terminal acetylation reduced H3K4 methylation, although this effect was only seen when the Set1-COMPASS protein Spp1 had also been lost (Figs. 4 and 5). Last, deleting the catalytic subunit of NatB reduced H3K4 methylation but only when Spp1 or Shg1 had also been removed. Moreover, blocking the N-terminal acetylation of Swd1 also reduced H3K4 methylation, although again only when *SPP1* had been deleted. Thus, NatB also regulates Set1-COMPASS activity likely via N-terminal acetylation of Swd1 (Fig. 6). These data together support the notion that NatA- and NatB-mediated N-terminal acetylation of Set1-COMPASS may shape its histone-methyltransferase activity (Fig. 7).

A crucial point is that deleting NatA activity has also been observed to reduce H2B ubiquitination and that this in turn decreases

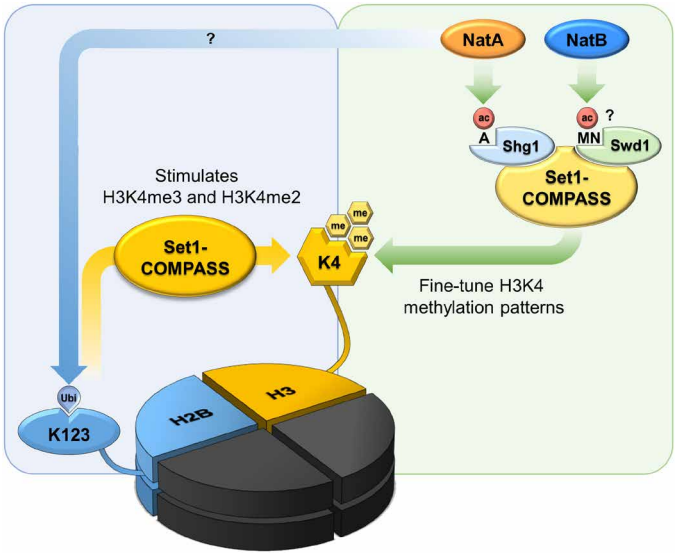

Fig. 7. Models for regulation of H3K4 methylation by N-terminal acetylation. H3K4 methylation mediated by Set1-COMPASS is enhanced by N-terminal acetylation through two distinct mechanisms. First, N-terminal acetylation by the N-terminal acetyltransferase NatA promotes proper Rad6/Bre1-mediated ubiquitination of histone H2B at K123 (H2B K123ub). This pathway is highlighted by the blue arrow. The NatA-target protein in this pathway is not clear. Proper H2B K123ub in turn promotes H3K4 methylation by Set1-COMPASS (yellow arrow). Second, NatA and NatB promote Set1-COMPASS-mediated H3K4 methylation by acetylating the N terminus of the Shg1 and Swd1 subunits, respectively (green arrow).

H3K4 methylation (*32*–*34*). Specifically, Rad6-Bre1–mediated H2B ubiquitination stimulates the generation of H3K4me3 and H3K4me2 by recruiting Set1-COMPASS to actively transcribed genes and/or via allosteric regulation of this complex (*37*–*39*). It has been shown that such H2B ubiquitination dependent H3K4 methylation requires a minimal complex consisting of Set1 and the WRAD components Bre2, Sdc1, Swd1, and Swd3 (*12*, *15*, *38*, *45*). Spp1 is also required for the H2B ubiquitination-dependent H3K4-methylation activity of Set1-COMPASS (*37*). Our present study confirmed that NatA deletion indeed impaired H2B ubiquitination (Fig. 1A). Therefore, we initially speculated that the suppressive effect of NatA deletion on Set1-COMPASS methyltransferase activity simply reflected poor H2B ubiquitination. However, two lines of evidence suggest that direct N-terminal acetylation of the Set1-COMPASS complex serves as an additional mechanism fine-tuning H3K4 methylation patterns. First, blocking Shg1 N-acetylation (in the context of Spp1 deletion) markedly reduced H3K4 methylation, and this effect did not associate with altered H2B ubiquitination (Fig. 5, A and C). Second, preventing the N-terminal acetylation of the NatB target Swd1 also decreased H3K4 methylation without affecting H2B ubiquitination (Fig. 6A and fig. S5A). Therefore, we propose that while optimal H3K4-methylation levels require histone cross-talk facilitated by H2B ubiquitination, and this cross-talk is driven by N-terminal acetylation of an as-yet unknown protein by NatA, N-terminal acetylation of Set1-COMPASS subunits by NatA and NatB also influences H3K4 methylation patterns (Fig. 7). In addition, it will be great interest to understand the mechanism by which NatA shapes Rad6-Bre1–mediated H2B ubiquitination.

N-terminal acetylation is an irreversible modification because enzymes that remove it have not been found. Consequently, this modification is not generally seen as a potential regulator of protein function. However, it is notable that N-terminal acetylome analyses in yeast show that 38% of NatA targets undergo partial acetylation (*35*). This coexistence of acetylated and unacetylated forms was also observed in Set1-COMPASS: Shg1, Spp1, and Swd2 underwent 57 to 80% N-terminal acetylation. Only the WRAD protein Swd1 exhibited 100% N-terminal acetylation (Fig. 3B). This together with our observation that N-terminal acetylation of Shg1 and Swd1 alters H3K4 methylation levels/patterns suggests that this modification can regulate Set1-COMPASS enzyme activity.

Different states of H3K4 methylation induced by the Set1-COMPASS regulate histone acetylation at distinct regions of genes. H3K4me3 enriched at active promoters serves as binding sites for the three yeast Inhibitor of Growth proteins Yng1, Yng2, and Pho23, which are respectively components of the NuA3 HAT, the NuA4 HAT, and the Rpd3 large (Rpd3L) HDAC, all of which act to optimize histone acetylation at promoters (*2*). H3K4me3 is also observed at active cryptic promoters within gene bodies and regulates noncoding RNA transcription (*5*, *46*, *47*). While the exact function of H3K4me1 enriched at 3′ regions of genes remains unclear, it is known that H3K4me2 peaking at 5′ transcribed regions functions as a binding site for Set3 HDAC to suppress a spreading of histone acetylation into gene bodies (*36*). While histone acetylation/deacetylation at the promoters has little effect on global transcript levels under steady-state growth conditions, it does influence the kinetics of gene induction or repression in response to environmental changes. In particular, H3K4me3 and its downstream effectors Yng1 and Pho23 regulate transcriptional repression memory (*46*, *48*), which facilitates faster gene repression when cells are re-exposed to the same or different stimuli. Our finding that N-terminal acetylation of Set1-COMPASS drives canonical H3K4 methylation patterns suggests that any derangement of NATs can lead to noncanonical patterns of H3K4 methylation: This in turn could induce the mislocalization of HATs and HDACs, thus disturbing the proper regulation of gene induction or repression kinetics. It is also possible that NATs can regulate histone acetylation patterns by directly shaping HAT and HDAC functions. Some components of these complexes are known to undergo N-terminal acetylation (*35*). In addition, as several elongation factors including Spt6 and Spt16 showed N-terminal acetylation, NATs may also affect transcription elongation by RNA Pol II resulting in noncanonical patterns of H3K4 methylation (*15*).

A question raised by our study was, how does N-terminal acetylation of Shg1 affect Set1-COMPASS function? N-terminal acetylation has been implicated in diverse regulatory functions, including enzyme activity and protein stability, localization, and complex formation (*25*). It also affects the functions of various chromatin modifiers and therefore plays a crucial role in regulating heterochromatic gene silencing. Specifically, NatA acetylates the N-terminal amino acid of the repressor protein origin recognition complex (ORC) and Sir3, a component of the Sir complex; these N-acetylation events are essential for the recruitment of ORC and Sir3 to silent HM (homothallic mating) loci. Once recruited, ORC binds to silencer elements while Sir3 contributes to the formation of heterochromatin structure (*49*–*52*). Moreover, Nat4-mediated N-terminal acetylation of histone H4 inhibits the dimethylation of H4R3 in in vitro histone methyltransferase assays (*53*). These observations

suggest that first-residue acetylation can modulate the structure of target proteins and thereby shape their interactions with chromatin or other proteins. We do not know how first-residue acetylation of Shg1 shapes Set1-COMPASS activity, but some possibilities can be excluded. First, it is unlikely that the N-terminal acetylation of Shg1 affects the enzyme activity of Set1-COMPASS because Kim *et al.* (*12*) showed that deleting Shg1 did not alter the histone-methyltransferase activity of purified Set1-COMPASS. Second, Shg1 N-terminal acetylation is unlikely to alter Set1-COMPASS composition: We found that deleting the catalytic subunit of NatA did not alter Set1-COMPASS assembly or the protein levels of the individual subunits (Fig. 1, E to G). Moreover, blocking N-terminal acetylation of Shg1 with the A2P mutation did not affect the protein levels of Shg1 and Set1 (Fig. 1G and fig. S4D). Third, Shg1 N-terminal acetylation is unlikely to affect the binding of Set1-COMPASS to active genes because we did not observe that loss of the NatA catalytic subunit had this effect (Fig. 1, C and D). Further studies are needed to unravel how N-terminal acetylation of Set1-COMPASS shapes its activity.

Our findings are relevant to humans because the NATs and Set1-containing complexes are evolutionally conserved from yeast to humans (*9*, *27*), and it has been shown that human NATs acetylate the Set1-COMPASS subunit homologs in the six human H3K4 methyltransferase complexes. Specifically, human NatA and NatB N-terminal acetylate WRAD components, namely, WDR5 (Swd3 in yeast), Ash2L (Bre2), and DPY30 (Sdc1) (*26*, *54*, *55*). Moreover, dysregulation of human NATs and the Set1-containing complexes associate with neurodegenerative diseases such as Parkinson's disease, Alzheimer's disease, and Huntington's disease (*56*, *57*). In particular, Alzheimer's disease has been linked with WDR5, which is a known substrate of human NatA (*58*, *59*). However, how N-terminal acetylation shapes the functions of these components in humans remains unknown. Thus, the fact that our study shows that N-terminal acetylation can regulate H3K4 methylation may help understand the disorders in humans that associate with defective H3K4 methyltransferase activity and N-terminal acetylation.

MATERIALS AND METHODS

Yeast strains

The yeast strains used in this study are listed in table S1. To generate the N-terminal substitution mutants, the *delitto-perfetto* strategy was used (*60*). The sequences of oligonucleotides used in this study are listed in table S2.

Western blot analysis

Cells were grown in yeast extract, peptone, and dextrose (YPD) to mid-log phase and lysed using lysis buffer [50 mM tris (pH 7.5), 150 mM NaCl, and 0.1% NP-40] with protease inhibitors [1 μM pepstatin A, 0.3 μM aprotinin, 1 μM leupeptin, and 1 mM phenylmethylsulfonyl fluoride (PMSF)] and glass beads. Protein concentration was determined with the Bradford assay. For SDS–polyacrylamide gel electrophoresis (SDS-PAGE) and Western blot analyses, 10 to 30 μg of whole-cell extracts were used. Proteins were separated by SDS-PAGE and transferred onto a nitrocellulose membrane (GE HealthCare). The blots were visualized on film with SuperSignal West Pico Chemiluminescent Substrate (Thermo Fisher Scientific). Anti-H3K4me3 (Millipore, 07-473), anti-H3K4me2 (Millipore, 07-030), anti-H3K4me1 (from A. Shilatifard, Northwestern University Feinberg School of Medicine), anti-H3 (Abcam, Ab1791), anti-H2Bub (Cell Signaling Technology, no. 5546), anti-H3K79me3 (Abcam, Ab2621), anti-Rpb3 (Biolegend, no. 665004), and anti-Set1 (Santa Cruz Biotechnology, sc-101858) were used for Western blot analysis.

TAP purification of Set1-COMPASS complex

The Bre2 component of COMPASS was TAP-tagged in wild-type, ard1Δ, and nat3Δ strains. The strains were cultured in 6 liters of YPD media and grown to an optical density at 600 nm (OD_{600}) of about 2.0. TAP purification was performed according to a previous study (*38*). Briefly, cells were resuspended with lysis buffer [for the final volume, 20 mM Hepes (pH 7.6), 10% glycerol, 250 mM NaCl, 0.1% Tween 20, 10 mM EDTA, 33 μM ZnOAc, freshly added 0.5 mM dithiothreitol (DTT), and 1X protease inhibitor] and lysed at an ice-cold bead beating homogenizer for 2 hours. The concentration of NaCl in cell extracts was adjusted to 200 mM. Cell extracts were precleared with 1 ml of Sepharose CL-4B (Sigma-Aldrich, no. CL4B200) at 4°C for 1 hour. Precleared cell extracts were incubated with 1 ml of IgG Sepharose (Cytiva, no. 17096901) at 4°C for 3 hours and washed with immunoglobulin G (IgG) binding buffer [20 mM Hepes (pH 7.6), 10% glycerol, 250 mM NaCl, 0.1% Tween 20, 10 mM EDTA, 100 μM ZnOAc, and freshly added 0.5 mM DTT]. The bound fractions were treated with a tobacco etch virus (TEV) protease (Biovision, no. 9205-1) and 1 ml of TEV cleavage buffer [10 mM tris (pH 8.0), 150 mM NaCl, 0.1% NP-40, 10% glycerol, 100 μM ZnOAc, and freshly added 0.5 mM DTT] at 4°C overnight rotating incubation. Elution fraction was collected, and the column was washed with 1 ml of calmodulin binding buffer [10 mM tris (pH 8.0), 150 mM NaCl, 0.1% NP-40, 10% glycerol, 100 μM ZnOAc, 1 mM MgOAc, 1 mM imidazole, 2 mM $CaCl_2$, and freshly added 10 mM β-mercaptoethanol]. The eluted and washed fractions were treated with 6.25 μl of 1 M $CaCl_2$ and incubated with calmodulin Sepharose (Cytiva, no. 17052901) at 4°C for 3 hours. The column was washed several times with calmodulin-binding buffer and eluted with calmodulin elution buffer (replaced the $CaCl_2$ of calmodulin-binding buffer with 2 mM EGTA). Eluted fractions were used for the LC-MS/MS.

Characterization of Set1-COMPASS composition and identification of N-terminal acetylated peptides by LC-MS/MS

Eluted samples were dried using Speed-Vac. Dried proteins were reconstructed with extraction buffer [1% SDS and 0.1 M DTT in 0.1 M tris (pH 8.0)]. After being heated at 95°C for 30 min, the denatured proteins were digested by a filter-aided sample preparation as described previously (*61*, *62*). Briefly, samples were loaded onto a 30K amicon filter (Millipore, Billerica, MA, USA), and buffer was exchanged with UA solution [8 M urea in 0.1 M tris-HCl (pH 8.5)] via centrifugation. After three buffer exchange with UA solution, the reduced cysteines were alkylated with 0.05 M iodoacetamide in UA solution for 30 min at room temperature in the dark. Thereafter. UA buffer was exchanged for 40 mM ammonium bicarbonate (ABC) twice. The protein samples were digested with trypsin/LysC (enzyme-to-substrate ratio of 1:100) at 37°C for 16 hours. The resulting peptides were collected in a new Eppendorf tube via centrifugation, and an additional elution step was performed using 40 mM ABC and 0.5 M NaCl. All resulting peptides were acidified with 10% trifluoroacetic acid and desalted using homemade C18-StageTips as described (*61*, *62*). Desalted peptides were completely dried with a vacuum dryer and stored at −80°C.

LC-MS/MS analysis was performed using an Orbitrap Exploris 480 mass spectrometer connected with Ultimate RSLC 3000 (Thermo Fisher Scientific, Bremen, Germany). Before sample injection, the dried peptide samples were redissolved in solvent A (2% acetonitrile and 0.1% formic acid). After the samples were loaded onto the nano LC, a 90-min gradient from 8 to 30% solvent B (100% acetonitrile and 0.1% formic acid) was applied to all samples. The mass spectrometer was operated in data-dependent mode with a full scan (mass/charge ratio 350 to 1650) followed by MS/MS for the top 15 precursor ions in each cycle. The acquired MS/MS spectra were subjected to searches against the Uniprot yeast database (UP000002311, 2022 April, 6650 entries) using SEQUEST-HT algorithm in Proteome Discoverer 3 (Thermo Fisher Scientific). Two missed trypsin cleavages were allowed, and the peptide mass tolerances for MS/MS and MS were set to 10 ppm and 0.02 Da, respectively. Other parameters used for the SEQUEST-HT searches included the fixed modification of carbamidomethylation at cysteine (+57.021 Da), the variable modification of oxidation at methionine (+15.995 Da), the N-terminal modification of acetylation at N terminus (42.011 Da), Met-loss at methionine (−131.040 Da) and Met-loss+acetylation at methionine (−89.030 Da). MS/MS spectra of Met-loss+acetylated peptides were manually validated to confirm peptide identification and Met-loss+acetylation site localization.

For the quantitative analyses of Set1-COMPASS composition in wild-type, *ard1*Δ, and *nat3*Δ strains, the spectral counts mapped to each protein were calculated. Following a methodology used in a prior study (*38*), we determined the NSAF (Normalized Spectral Associated Factor) values for COMPASS components using spectral counts (*63*). Subsequently, we normalized these values by dividing them by the NSAF value corresponding to Set1. This approach allowed us to compare the assembly of Set1-COMPASS purified from wild-type, *ard1*Δ, and *nat3*Δ strains.

Silver staining

Eluates obtained from the two-step TAP purification of Bre2-TAP in both wild-type and *ard1*Δ strains were subjected to SDS-PAGE gel separation. The gel was fixed for 1 hour in a fixative solution [30% ethanol and 10% acetic acid in deionized water (DIW)] on a shaker. Subsequently, the gel was rinsed in 20% ethanol for 20 min, sensitized by immersion in 0.02% sodium thiosulfate for 2 min, and then washed with DIW for 20 s three times. The gel was incubated in 0.2% silver nitrate for 1 hour on the shaker, washed with DIW for 30 s three times, and then developed using 50 ml of developing solution (1.5 g of sodium carbonate, 2.5 ml of 0.02% sodium thiosulfate, 50 μl of formaldehyde, and DIW up to 50 ml).

Coimmunoprecipitations

Whole-cell extracts were prepared with binding buffer containing 50 mM tris-HCl (pH 7.5), 0.1% NP-40, 225 mM NaCl, and protease inhibitors (1 μM pepstatin A, 0.3 μM aprotinin, 1 μM leupeptin, and 1 mM PMSF). For Fig. 1G, 1 mg of whole-cell extracts were incubated with ProteinG sepharose (GE HealthCare, 17-0618-01) and anti-Myc (Biolegend, no. 626802) at 4°C for 4 hours, and then the beads were washed with binding buffer. The precipitates were resolved by SDS-PAGE followed by immunoblot analysis. For Fig. 3C, 25 mg of whole-cell extracts was incubated with IgG Sepharose (GE HealthCare, 17078001), and after washing, the bead-bound complexes were treated with 30 U of TEV protease and 40 ml of TEV cleavage buffer. The eluates were resolved by SDS-PAGE followed by immunoblot analysis.

ChIP assay and ChIP-seq

The ChIP assays were performed as described previously (*36*) with the oligonucleotides shown in table S2. The yeast strains for these assays were cultured in 200 ml of media at 30°C until they reached an OD_{600} of 0.5. Formaldehyde was added to a final concentration of 1% for cross-linking, and the cells were incubated for 20 min at room temperature. Cross-linking was quenched with 3 M glycine for 5 min at room temperature. The cell pellets were then recovered, washed with FA buffer [50 mM Hepes-KOH (pH 7.5), 150 mM NaCl, 1 mM EDTA, 1% Triton X-100, 0.1% sodium deoxycholate, and 0.1% SDS], resuspended in FA buffer/0.5% SDS with glass beads, and lysed through a series of vortexing and cooling steps. The cell lysates were separated from the beads through centrifugation, and the supernatants were sonicated using a Branson digital sonifier (S-450D). Centrifugation was then used to separate the insoluble fraction from the soluble chromatin. The protein in the supernatant was quantified using a Bradford assay. ChIP assays were conducted with 250 μg of chromatin, specific antibodies, and beads, namely, 1 μl of anti-H3 (Abcam, Ab1791), 0.5 μl of anti-H3K4me2 (Millipore, 07-030), or 0.5 μl of anti-H3K4me3 (Millipore, 07-473) bound to Protein A Sepharose (GE HealthCare, 17078001); 2 μl of anti-Rpb3 (Neoclone) bound to Protein G Sepharose (GE HealthCare, 17061801); 2 μl of anti-HA (Santa Cruz Biotechnology, sc-7392) bound to Protein A/G PLUS-Agarose (Santa Cruz Biotechnology, sc-2003); and IgG bead (GE HealthCare, no. 17-0969-01) for TAP-tagged proteins. Antibody binding was achieved overnight in FA lysis buffer containing different concentrations of NaCl depending on the antibody. The precipitates were then washed with FA lysis buffer and then with a third wash buffer [10 mM tris-HCl (pH 8.0), 0.25 M LiCl, 1 mM EDTA, 0.5% NP-40, and 0.5% sodium deoxycholate]. After the wash process, the immunoprecipitates were eluted with elution buffer [50 mM tris-HCl (pH7.5), 10 mM EDTA, and 1% SDS] at 65°C for 20 min. DNA precipitation was then conducted as described (*36*), and the precipitated DNAs were subjected to real-time quantitative polymerase chain reaction (qPCR) using a CFX96 cycler (Bio-Rad) and SYBR qPCR Master Mix (TOYOBO, QPX-201). ChIP-seq was conducted the same way but with double the quantities of all inputs and with *S. pombe* chromatin representing 10% of the *Saccharomyces cerevisiae* chromatin. For ChIP-seq, DNA libraries were prepared and sequenced on the Illumina platform.

ChIP-seq data analysis

Trimmomatic v.0.36 performed the sequencing adapter removal and quality-based trimming of raw data with TruSeq adapter sequences (*64*). Cleaned reads were mapped to the reference genome using bowtie2 v.2.2.5 with the default parameter (*65*). ChIP-seq reads were allocated to the genome of *S. cerevisiae* or *S. pombe*, and normalization factors were determined by adjusting the *S. pombe* reads of each sample to 1 million reads (*15*). Resulted BedGraph files were used as the input data for EaSeq (http://easeq.net) or IGV (*66*, *67*). The total yeast genes ($n = 6020$) were then selected with the following procedures. First, 7105 genes were isolated after excluding noncoding exons from the 7589-gene sacCer3 reference genome (UniProt, 07/15/2017 version). Protein-coding genes without repetition ($n = 6020$) were then selected for the ChIP-seq data analysis. After calculating the mean RPM (reads per million) values of Set1-3X HA, Set1-TAP, H3K4me2, H3K4me3, and H3 of each gene, heatmaps and anchor plots were drawn with the guidance of EaSeq. To draw the heatmaps, the genes were sorted according to the mean RPM value of H3K4me3 of the wild-type strain mapped from −100 to +300 bp of TSS. To draw

the scatter plots in Fig. 2D, the mapped reads of H3K4me2 and H3K4me3 in the promoter region (from −100 to +300 bp based on TSS) were quantified by the quantification tool in EaSeq and normalized by the value of H3. The genes whose H3K4me2 levels in the promoter rose or fell when *ARD1* was deleted were then identified: They were designated the H3K4me2^{incr} group ($n = 4093$) and H3K4me2^{decr} group ($n = 1905$), respectively.

Supplementary Materials

This PDF file includes:

Figs. S1 to S5
Tables S1 and S2

REFERENCES AND NOTES

1. B. Li, M. Carey, J. L. Workman, The role of chromatin during transcription. *Cell* **128**, 707–719 (2007).
2. H. Woo, S. Dam Ha, S. B. Lee, S. Buratowski, T. Kim, Modulation of gene expression dynamics by co-transcriptional histone methylations. *Exp. Mol. Med.* **49**, e326 (2017).
3. T. Kim, Z. Xu, S. Clauder-Munster, L. M. Steinmetz, S. Buratowski, Set3 HDAC mediates effects of overlapping noncoding transcription on gene induction kinetics. *Cell* **150**, 1158–1169 (2012).
4. S. D. Ha, S. Ham, M. Y. Kim, J. H. Kim, I. Jang, B. B. Lee, M. K. Lee, J. T. Hwang, T. Y. Roh, T. Kim, Transcription-dependent targeting of Hda1C to hyperactive genes mediates H4-specific deacetylation in yeast. *Nat. Commun.* **10**, 4270 (2019).
5. J. H. Kim, B. B. Lee, Y. M. Oh, C. Zhu, L. M. Steinmetz, Y. Lee, W. K. Kim, S. B. Lee, S. Buratowski, T. Kim, Modulation of mRNA and lncRNA expression dynamics by the Set2-Rpd3S pathway. *Nat. Commun.* **7**, 13534 (2016).
6. T. Miller, N. J. Krogan, J. Dover, H. Erdjument-Bromage, P. Tempst, M. Johnston, J. F. Greenblatt, A. Shilatifard, COMPASS: A complex of proteins associated with a trithorax-related SET domain protein. *Proc. Natl. Acad. Sci. U.S.A.* **98**, 12902–12907 (2001).
7. A. Roguev, D. Schaft, A. Shevchenko, W. W. Pijnappel, M. Wilm, R. Aasland, A. F. Stewart, The Saccharomyces cerevisiae Set1 complex includes an Ash2 homologue and methylates histone 3 lysine 4. *EMBO J.* **20**, 7137–7148 (2001).
8. N. J. Krogan, J. Dover, S. Khorrami, J. F. Greenblatt, J. Schneider, M. Johnston, A. Shilatifard, COMPASS, a histone H3 (Lysine 4) methyltransferase required for telomeric silencing of gene expression. *J. Biol. Chem.* **277**, 10753–10755 (2002).
9. J. C. Eissenberg, A. Shilatifard, Histone H3 lysine 4 (H3K4) methylation in development and differentiation. *Dev. Biol.* **339**, 240–249 (2010).
10. F. S. Howe, H. Fischl, S. C. Murray, J. Mellor, Is H3K4me3 instructive for transcription activation? *Bioessays* **39**, 1–12 (2017).
11. P. Ernst, C. R. Vakoc, WRAD: Enabler of the SET1-family of H3K4 methyltransferases. *Brief. Funct. Genomics* **11**, 217–226 (2012).
12. J. Kim, J. A. Kim, R. K. McGinty, U. T. Nguyen, T. W. Muir, C. D. Allis, R. G. Roeder, The n-SET domain of Set1 regulates H2B ubiquitylation-dependent H3K4 methylation. *Mol. Cell* **49**, 1121–1133 (2013).
13. H. J. Bae, M. Dubarry, J. Jeon, L. M. Soares, C. Dargemont, J. Kim, V. Geli, S. Buratowski, The Set1 N-terminal domain and Swd2 interact with RNA polymerase II CTD to recruit COMPASS. *Nat. Commun.* **11**, 2181 (2020).
14. H. H. Ng, F. Robert, R. A. Young, K. Struhl, Targeted recruitment of Set1 histone methylase by elongating Pol II provides a localized mark and memory of recent transcriptional activity. *Mol. Cell* **11**, 709–719 (2003).
15. L. M. Soares, P. C. He, Y. Chun, H. Suh, T. Kim, S. Buratowski, Determinants of histone H3K4 methylation patterns. *Mol. Cell* **68**, 773–785.e6 (2017).
16. J. Dover, J. Schneider, M. A. Tawiah-Boateng, A. Wood, K. Dean, M. Johnston, A. Shilatifard, Methylation of histone H3 by COMPASS requires ubiquitination of histone H2B by Rad6. *J. Biol. Chem.* **277**, 28368–28371 (2002).
17. Z. W. Sun, C. D. Allis, Ubiquitination of histone H2B regulates H3 methylation and gene silencing in yeast. *Nature* **418**, 104–108 (2002).
18. R. N. Laribee, N. J. Krogan, T. Xiao, Y. Shibata, T. R. Hughes, J. F. Greenblatt, B. D. Strahl, BUR kinase selectively regulates H3 K4 trimethylation and H2B ubiquitylation through recruitment of the PAF elongation complex. *Curr. Biol.* **15**, 1487–1493 (2005).
19. K. W. Mulder, A. B. Brenkman, A. Inagaki, N. J. van den Broek, H. T. Timmers, Regulation of histone H3K4 tri-methylation and PAF complex recruitment by the Ccr4-Not complex. *Nucleic Acids Res.* **35**, 2428–2439 (2007).
20. V. E. Maltby, B. J. Martin, J. Brind'Amour, A. T. Chruscicki, K. L. McBurney, J. M. Schulze, I. J. Johnson, M. Hills, T. Hentrich, M. S. Kobor, M. C. Lorincz, L. J. Howe, Histone H3K4 demethylation is negatively regulated by histone H3 acetylation in Saccharomyces cerevisiae. *Proc. Natl. Acad. Sci. U.S.A.* **109**, 18505–18510 (2012).
21. C. K. Govind, F. Zhang, H. Qiu, K. Hofmeyer, A. G. Hinnebusch, Gcn5 promotes acetylation, eviction, and methylation of nucleosomes in transcribed coding regions. *Mol. Cell* **25**, 31–42 (2007).
22. A. Kirmizis, H. Santos-Rosa, C. J. Penkett, M. A. Singer, M. Vermeulen, M. Mann, J. Bahler, R. D. Green, T. Kouzarides, Arginine methylation at histone H3R2 controls deposition of H3K4 trimethylation. *Nature* **449**, 928–932 (2007).
23. C. C. Yuan, A. G. Matthews, Y. Jin, C. F. Chen, B. A. Chapman, T. K. Ohsumi, K. C. Glass, T. G. Kutateladze, M. L. Borowsky, K. Struhl, M. A. Oettinger, Histone H3R2 symmetric dimethylation and histone H3K4 trimethylation are tightly correlated in eukaryotic genomes. *Cell Rep.* **1**, 83–90 (2012).
24. H. Aksnes, A. Drazic, M. Marie, T. Arnesen, First things first: Vital protein marks by N-terminal acetyltransferases. *Trends Biochem. Sci.* **41**, 746–760 (2016).
25. R. Ree, S. Varland, T. Arnesen, Spotlight on protein N-terminal acetylation. *Exp. Mol. Med.* **50**, 1–13 (2018).
26. P. Van Damme, K. Hole, A. Pimenta-Marques, K. Helsens, J. Vandekerckhove, R. G. Martinho, K. Gevaert, T. Arnesen, NatF contributes to an evolutionary shift in protein N-terminal acetylation and is important for normal chromosome segregation. *PLOS Genet.* **7**, e1002169 (2011).
27. T. Arnesen, P. Van Damme, B. Polevoda, K. Helsens, R. Evjenth, N. Colaert, J. E. Varhaug, J. Vandekerckhove, J. R. Lillehaug, F. Sherman, K. Gevaert, Proteomics analyses reveal the evolutionary conservation and divergence of N-terminal acetyltransferases from yeast and humans. *Proc. Natl. Acad. Sci. U.S.A.* **106**, 8157–8162 (2009).
28. H. Aksnes, K. Hole, T. Arnesen, Molecular, cellular, and physiological significance of N-terminal acetylation. *Int. Rev. Cell Mol. Biol.* **316**, 267–305 (2015).
29. E. Linster, M. Wirtz, N-terminal acetylation: An essential protein modification emerges as an important regulator of stress responses. *J. Exp. Bot.* **69**, 4555–4568 (2018).
30. K. K. Starheim, K. Gevaert, T. Arnesen, Protein N-terminal acetyltransferases: When the start matters. *Trends Biochem. Sci.* **37**, 152–161 (2012).
31. C. Feller, I. Forne, A. Imhof, P. B. Becker, Global and specific responses of the histone acetylome to systematic perturbation. *Mol. Cell* **57**, 559–571 (2015).
32. L. Jiang, J. N. Smith, S. L. Anderson, P. Ma, C. A. Mizzen, N. L. Kelleher, Global assessment of combinatorial post-translational modification of core histones in yeast using contemporary mass spectrometry. LYS4 trimethylation correlates with degree of acetylation on the same H3 tail. *J. Biol. Chem.* **282**, 27923–27934 (2007).
33. Y. H. Takahashi, J. M. Schulze, J. Jackson, T. Hentrich, C. Seidel, S. L. Jaspersen, M. S. Kobor, A. Shilatifard, Dot1 and histone H3K79 methylation in natural telomeric and HM silencing. *Mol. Cell* **42**, 118–126 (2011).
34. H. Vlaming, T. M. Molenaar, T. van Welsem, D. W. Poramba-Liyanage, D. E. Smith, A. Velds, L. Hoekman, T. Korthout, S. Hendriks, A. F. M. Altelaar, F. van Leeuwen, Direct screening for chromatin status on DNA barcodes in yeast delineates the regulome of H3K79 methylation by Dot1. *eLife* **5**, e18919 (2016).
35. P. Van Damme, S. I. Stove, N. Glomnes, K. Gevaert, T. Arnesen, A *Saccharomyces cerevisiae* model reveals in vivo functional impairment of the Ogden syndrome N-terminal acetyltransferase NAA10 Ser37Pro mutant. *Mol. Cell. Proteomics* **13**, 2031–2041 (2014).
36. T. Kim, S. Buratowski, Dimethylation of H3K4 by Set1 recruits the Set3 histone deacetylase complex to 5′ transcribed regions. *Cell* **137**, 259–272 (2009).
37. J. Jeon, R. K. McGinty, T. W. Muir, J. A. Kim, J. Kim, Crosstalk among Set1 complex subunits involved in H2B ubiquitylation-dependent H3K4 methylation. *Nucleic Acids Res.* **46**, 11129–11143 (2018).
38. J. S. Lee, A. Shukla, J. Schneider, S. K. Swanson, M. P. Washburn, L. Florens, S. R. Bhaumik, A. Shilatifard, Histone crosstalk between H2B monoubiquitination and H3 methylation mediated by COMPASS. *Cell* **131**, 1084–1096 (2007).
39. A. Vitaliano-Prunier, A. Menant, M. Hobeika, V. Geli, C. Gwizdek, C. Dargemont, Ubiquitylation of the COMPASS component Swd2 links H2B ubiquitylation to H3K4 trimethylation. *Nat. Cell Biol.* **10**, 1365–1371 (2008).
40. D. P. Mersman, H. N. Du, I. M. Fingerman, P. F. South, S. D. Briggs, Charge-based interaction conserved within histone H3 lysine 4 (H3K4) methyltransferase complexes is needed for protein stability, histone methylation, and gene expression. *J. Biol. Chem.* **287**, 2652–2665 (2012).
41. L. M. Soares, M. Radman-Livaja, S. G. Lin, O. J. Rando, S. Buratowski, Feedback control of Set1 protein levels is important for proper H3K4 methylation patterns. *Cell Rep.* **6**, 961–972 (2014).
42. J. E. Mueller, M. Canze, M. Bryk, The requirements for COMPASS and Paf1 in transcriptional silencing and methylation of histone H3 in Saccharomyces cerevisiae. *Genetics* **173**, 557–567 (2006).
43. B. Polevoda, F. Sherman, Nalpha-terminal acetylation of eukaryotic proteins. *J. Biol. Chem.* **275**, 36479–36482 (2000).
44. S. Huang, R. C. Elliott, P. S. Liu, R. K. Koduri, J. L. Weickmann, J. H. Lee, L. C. Blair, P. Ghosh-Dastidar, R. A. Bradshaw, K. M. Bryan, B. Einarson, R. L. Kendall, K. H. Kolacz, K. Saito, Specificity of cotranslational amino-terminal processing of proteins in yeast. *Biochemistry* **26**, 8242–8246 (1987).

45. A. Shilatifard, The COMPASS family of histone H3K4 methylases: Mechanisms of regulation in development and disease pathogenesis. *Annu. Rev. Biochem.* **81**, 65–95 (2012).
46. J. H. Kim, C. Y. Yoon, Y. Jun, B. B. Lee, J. E. Lee, S. D. Ha, H. Woo, A. Choi, S. Lee, W. Jeong, J. H. Kim, T. Kim, NuA3 HAT antagonizes the Rpd3S and Rpd3L HDACs to optimize mRNA and lncRNA expression dynamics. *Nucleic Acids Res.* **48**, 10753–10767 (2020).
47. B. B. Lee, H. Woo, M. K. Lee, S. Youn, S. Lee, J. S. Roe, S. Y. Lee, T. Kim, Core promoter activity contributes to chromatin-based regulation of internal cryptic promoters. *Nucleic Acids Res.* **49**, 8097–8109 (2021).
48. B. B. Lee, A. Choi, J. H. Kim, Y. Jun, H. Woo, S. D. Ha, C. Y. Yoon, J. T. Hwang, L. Steinmetz, S. Buratowski, S. Lee, H. Y. Kim, T. Kim, Rpd3L HDAC links H3K4me3 to transcriptional repression memory. *Nucleic Acids Res.* **46**, 8261–8274 (2018).
49. S. Kueng, M. Oppikofer, S. M. Gasser, SIR proteins and the assembly of silent chromatin in budding yeast. *Annu. Rev. Genet.* **47**, 275–306 (2013).
50. A. Geissenhoner, C. Weise, A. E. Ehrenhofer-Murray, Dependence of ORC silencing function on NatA-mediated N^{α} acetylation in *Saccharomyces cerevisiae*. *Mol. Cell. Biol.* **24**, 10300–10312 (2004).
51. M. Onishi, G. G. Liou, J. R. Buchberger, T. Walz, D. Moazed, Role of the conserved Sir3-BAH domain in nucleosome binding and silent chromatin assembly. *Mol. Cell* **28**, 1015–1028 (2007).
52. T. van Welsem, F. Frederiks, K. F. Verzijlbergen, A. W. Faber, Z. W. Nelson, D. A. Egan, D. E. Gottschling, F. van Leeuwen, Synthetic lethal screens identify gene silencing processes in yeast and implicate the acetylated amino terminus of Sir3 in recognition of the nucleosome core. *Mol. Cell. Biol.* **28**, 3861–3872 (2008).
53. V. Schiza, D. Molina-Serrano, D. Kyriakou, A. Hadjiantoniou, A. Kirmizis, N-alpha-terminal acetylation of histone H4 regulates arginine methylation and ribosomal DNA silencing. *PLOS Genet.* **9**, e1003805 (2013).
54. P. Van Damme, M. Lasa, B. Polevoda, C. Gazquez, A. Elosegui-Artola, D. S. Kim, E. De Juan-Pardo, K. Demeyer, K. Hole, E. Larrea, E. Timmerman, J. Prieto, T. Arnesen, F. Sherman, K. Gevaert, R. Aldabe, N-terminal acetylome analyses and functional insights of the N-terminal acetyltransferase NatB. *Proc. Natl. Acad. Sci. U.S.A.* **109**, 12449–12454 (2012).
55. P. Van Damme, K. Hole, K. Gevaert, T. Arnesen, N-terminal acetylome analysis reveals the specificity of Naa50 (Nat5) and suggests a kinetic competition between N-terminal acetyltransferases and methionine aminopeptidases. *Proteomics* **15**, 2436–2446 (2015).
56. Y. Wu, G. J. Lyon, NAA10-related syndrome. *Exp. Mol. Med.* **50**, 1–10 (2018).
57. B. S. Basavarajappa, S. Subbanna, Histone Methylation Regulation in Neurodegenerative Disorders. *Int. J. Mol. Sci.* **22**, (2021).
58. Q. Liu, X. Liu, D. Zhao, X. Ruan, R. Su, X. Shang, D. Wang, C. Yang, Y. Xue, Pseudogene ACTBP2 increases blood-brain barrier permeability by promoting KHDRBS2 transcription through recruitment of KMT2D/WDR5 in $A\beta_{1-42}$ microenvironment. *Cell Death Discov.* **7**, 142 (2021).
59. Q. Cao, W. Wang, J. B. Williams, F. Yang, Z. J. Wang, Z. Yan, Targeting histone K4 trimethylation for treatment of cognitive and synaptic deficits in mouse models of Alzheimer's disease. *Sci. Adv.* **6**, eabc8096 (2020).
60. F. Storici, M. A. Resnick, The delitto perfetto approach to in vivo site-directed mutagenesis and chromosome rearrangements with synthetic oligonucleotides in yeast. *Methods Enzymol.* **409**, 329–345 (2006).
61. H. Kim, J. Woo, K. Dan, K. M. Lee, M. S. Jin, I. A. Park, H. S. Ryu, D. Han, Quantitative proteomics reveals knockdown of CD44 promotes proliferation and migration in claudin-low MDA-MB-231 and Hs 578T breast cancer cell lines. *J. Proteome Res.* **20**, 3720–3733 (2021).
62. S. H. Kong, J. H. Lee, J. M. Bae, N. Hong, H. Kim, S. Y. Park, Y. J. Choi, S. Lee, Y. Rhee, S. W. Kim, D. Han, J. H. Kim, C. S. Shin, In-depth proteomic signature of parathyroid carcinoma. *Eur. J. Endocrinol.* **188**, 385–394 (2023).
63. B. Zybailov, A. L. Mosley, M. E. Sardiu, M. K. Coleman, L. Florens, M. P. Washburn, Statistical analysis of membrane proteome expression changes in Saccharomyces cerevisiae. *J. Proteome Res.* **5**, 2339–2347 (2006).
64. A. M. Bolger, M. Lohse, B. Usadel, Trimmomatic: A flexible trimmer for Illumina sequence data. *Bioinformatics* **30**, 2114–2120 (2014).
65. B. Langmead, S. L. Salzberg, Fast gapped-read alignment with Bowtie 2. *Nat. Methods* **9**, 357–359 (2012).
66. M. Lerdrup, J. V. Johansen, S. Agrawal-Singh, K. Hansen, An interactive environment for agile analysis and visualization of ChIP-sequencing data. *Nat. Struct. Mol. Biol.* **23**, 349–357 (2016).
67. K. A. Robinson, I. J. Saldanha, N. A. McKoy, Development of a framework to identify research gaps from systematic reviews. *J. Clin. Epidemiol.* **64**, 1325–1330 (2011).

Acknowledgments: We thank all members of the Kim laboratory and the Lee laboratory for helpful advice and discussions. **Funding:** This work was supported by grants from the National Research Foundation (NRF-2022R1A2C3005694 and RS-2023-00217798 to T.K., NRF-2020R1I1A3072234 and NRF-2023R1A2C1003170 to J.-S.L., and NRF-2020R1A6A3A13077356 and NRF-2022R1A6A3A01087657 to J.O.) and grant from the Korea Basic Science Institute (National Research Facilities and Equipment Center) funded by the Ministry of Education (2019R1A6C1010020) to T.K. Funding for open-access charge: National Research Foundation.
Author contributions: Conceptualization: H.W., G.T.O., T.K., and J.-S.L. Methodology: H.W., J.O., Y.-J.C., and G.T.O. Investigation: H.W., J.O., Y.-J.C., K.D., D.H., and S.-Y.K. Visualization: H.W., J.O., and T.K. Supervision: T.K. and J.-S.L. Writing—original draft: H.W., J.O., K.D., J.-S.L., and T.K. Writing—review and editing: H.W., J.O., D.H., J.-S.L., and T.K. **Competing interests:** The authors declare that they have no competing interests. **Data and materials availability:** All data needed to evaluate the conclusions in the paper are present in the paper and/or the Supplementary Materials. The accession code for ChIP-seq data of H3K4 methylation and Set1, generated in this study, has been deposited in the GEO database under accession number GSE238070.

Submitted 2 November 2023
Accepted 7 June 2024
Published 12 July 2024
10.1126/sciadv.adl6280